LANGMUIR

pubs.acs.org/Langmuir Article

A *Phyllostachys Edulis*-Derived Microporous Carbon-Coated Separator with Improved Li^+ Transport for Long Cycling Lithium−Chalcogenide Batteries

Panpan Dong, Ting Yang, Xuemeng Gan, Xing Liu,* and Weiqing Yang*

Cite This: *Langmuir* 2026, 42, 24682−24690 Read Online

ACCESS | Metrics & More | Article Recommendations | Supporting Information

ABSTRACT: Lithium−chalcogenide batteries (LCBs) offer high theoretical energy density but suffer from the polysulfide/polyselenide shuttling during charging and discharging processes with conventional polypropylene (PP) separators, causing low active-material utilization and severe capacity decay. Herein, we develop a *Phyllostachys edulis* bamboo-derived microporous carbon-coated PP separator (MPC@PP) to suppress polychalcogenide migration and enable long-term cycling. The abundant micropores in the MPC coating enhance polysulfide adsorption and boost the Li^+ transference number to 0.57, which is a 46.2% increase over pristine PP (0.39). The lithium symmetric Li/Li cell with MPC@PP exhibits good cycling stability up to 300 h at 0.5 mA cm^{-2} (1 mAh cm^{-2}) with a smooth and compact lithium deposition. When used in Li−S battery with the S@Ketjenblack cathode, the MPC@PP cell delivers a reversible capacity of 1272.92 mAh g^{-1} at 167.5 mA g^{-1} and stable cycling over 500 cycles at 837.5 mA g^{-1}. Moreover, Li−SeS_2 battery with MPC@PP achieves an initial capacity of 723.48 mAh g^{-1} at 1342 mA g^{-1} with average Coulombic efficiency >99.2% for 500 cycles. This work provides a cost-effective and scalable biomass-derived microporous carbon strategy to address the critical challenges of LCBs, offering valuable guidance for advanced separator design and accelerating the deployment of high-energy-density rechargeable batteries.



INTRODUCTION

Lithium−chalcogenide batteries (LCBs), primarily including lithium−sulfur (Li−S), lithium−selenium (Li−Se), and lithium−selenium disulfide (Li−SeS_2) systems, show great potential as next-generation high-energy-density storage devices owing to their high theoretical specific energy, low cost, and environmental friendliness.[1−4] Despite these merits, their practical application is hindered by several intrinsic challenges arising from the properties of chalcogens (S, Se, etc.) and their discharge products.[5−9] The key issues include the poor electronic conductivity and the shuttling of dissolved polysulfides/polyselenides in the electrolyte, and the uniform lithium deposition, resulting in poor utilization of cathodes and fast capacity loss during long cycling.

In batteries, the separator plays a critical role in preventing direct electrode contact to avoid short circuits while providing essential pathways for ion conduction.[10,11] Conventional polyolefin separators, although facilitating Li^+ transport through their porous structure, offer no barrier to the migration of polychalcogenides in LCBs. The polychalcogenide ions that reach the anode react with the lithium metal surface, forming insoluble deposits. These deposits not only aggravate anode passivation and polarization but also directly cause irreversible active material loss and rapid capacity fading. Moreover, conventional porous separators are incapable of regulating the lithium-ion transference number (typically <0.4) of the electrolyte,[12−14] leading to inhomogeneous lithium deposition and consequently low reversibility of the lithium metal anode. As a result, these separators cannot effectively mitigate the shuttling of polychalcogenides, thus failing to prevent the degradation of active materials and the corrosion of the lithium anode.

In recent years, separator modification with various functional materials,[15,16] including carbonaceous materials,[17−19] transition-metal compounds,[20,21] metal−organic frameworks,[22−25] covalent−organic frameworks,[26,27] polymers,[28,29] and high-dielectric ceramics,[30,31] has been extensively explored to suppress the shuttle effect and stabilize lithium anodes in Li−S and Li−Se batteries. Among them, carbon-based interlayers,[32−34] particularly porous carbons,[35] remain the most foundational and widely studied platform because of their good conductivity, tunable porosity, and physical/chemical barrier capabilities. For example, Srikhaow et al.[36] demonstrated that a hydrothermally synthesized nitrogen-doped reduced graphene oxide coating on a

Received: July 6, 2026
Revised: July 31, 2026
Accepted: August 2, 2026
Published: August 8, 2026



Downloaded from pubs.acs.org/langd5/article-pdf/42/33/24682/6646793/acs.langmuir.6c04214.pdf by SOUTHWEST JIAOTONG UNIV user on 07 November 2026

© 2026 American Chemical Society

https://doi.org/10.1021/acs.langmuir.6c04214
Langmuir 2026, 42, 24682−24690

commercial PP separator effectively suppressed polysulfide diffusion through strong chemical affinity between polysulfides and nitrogen sites, delivering an initial capacity of 1563 mAh g^{-1} at 0.1C with 83.7% capacity retention after 200 cycles. In 2023, Jo et al.[37] developed a biomass-derived activated carbon from milk waste via a facile one-pot synthesis and combined it with an Al_2O_3 ceramic layer on a PE separator, achieving a discharge capacity of 1092.5 mAh g^{-1} at 0.1C while simultaneously suppressing lithium dendrite growth. More recently, Kang et al.[38] utilized MOF-derived porous carbons with precisely tuned pore sizes as separator coatings and identified that a pore size of 0.8 nm provided an optimal ion-sieving effect, effectively blocking polysulfide migration while promoting Li^+ diffusion, thereby enabling stable long-term cycling. Despite these advances, the fabrication of most high-performance porous carbon modifiers typically relies on precisely engineered pore structures via multistep, high-cost synthetic methods, such as template-assisted carbonization,[39] chemical vapor deposition,[40] or multistep composite engineering,[41] which involve costly precursors, high energy consumption, and limited scalability. These inherent drawbacks severely impede their practical implementation and large-scale production. Consequently, there is an urgent and compelling need to develop low-cost, easily processable, yet highly effective porous carbon materials for separator modification, with the aim of achieving a practical balance between electrochemical performance, manufacturing simplicity, and economic viability.

Herein, to address the urgent need for low-cost and scalable porous carbon-modified separator, we present an optimized microporous carbon derived from *Phyllostachys edulis* bamboo at different temperatures (denoted as *x*-MPC, *x* = 400, 500, and 600 °C) as a functional separator coating for high-performance lithium−chalcogenide batteries (LCBs). We demonstrate that this porous carbon coating plays a crucial role in mitigating the shuttle effect of redox intermediates. The abundant micropores in the coating can physically mitigate polysulfide/polyselenide shuttling as well as homogenize the Li^+ flux, enabling smooth and compact dendrite-free lithium deposition. Compared with the pristine PP separator, LCBs using the 500-MPC@PP separator exhibit significantly improved cycling stability and rate performance. Benefiting from the effective polychalcogenide barrier provided by the microporous carbon, the 500-MPC@PP-based Li−S battery using the S@Ketjenblack cathode delivers a high initial specific capacity of 1272.92 mAh g^{-1} at 167.5 mA g^{-1} and good cycling stability up to 500 cycles at 837.5 mA g^{-1}. Moreover, Li−SeS_2 battery with such 500-MPC@PP separator exhibits much enhanced cycling stability with a Coulombic efficiency of 99.2% over 500 cycles at 1342 mA g^{-1}. This work demonstrates that the *P. edulis*-derived microporous carbon separator can achieve superior capacity and stability, offering valuable insights for designing lithium−chalcogenide batteries with enhanced performances.

EXPERIMENTAL SECTION

Materials and Chemicals

Sublimed sulfur (S, >99.5%) was purchased from Kermel. Ketjenblack (KB, EC-600JD), polyvinylidene difluoride (PVDF), and conductive carbon (Super-C45) were obtained from Canrd Technology Co., Ltd. Lithium bis(trifluoromethanesulfonyl)imide (LiTFSI, 99.99%) and selenium disulfide (SeS_2, 97%) were supplied by MACKLIN. *N*-methylpyrrolidone (NMP, >99%), 1,2-dimethoxyethane (DME, >99.5%), lithium sulfide (Li_2S, >99.98%), 1,3-dioxolane (DOL, >99.8%), and lithium nitrate ($LiNO_3$, >99.99%) were obtained from Aladdin. Lithium chips with a diameter of 15.6 mm and thickness of 450 μm) were provided from NEWARE. The PP separator (Celgard 2400) was supplied by Celgard.

Synthesis of S, S@KB, and SeS_2@KB Cathodes

The pristine S electrode was prepared according to a previous report.[42] The active material loading in the obtained electrode was 1.6−2.0 mg cm^{-2}. The same method was used to prepare S@KB and SeS_2@KB electrodes. In the composite electrodes, the mass ratio between S (or SeS_2) and KB was 7:3. The mass ratio between active material, conductive carbon, and binder was controlled as 7:2:1. The mass loading of S (or SeS_2) in composite electrodes was 1.0−1.2 mg cm^{-2}. All electrodes were cut into round shape with a diameter of 12 mm before use.

Synthesis of 500-MPC and 500-MPC-Coated Separator

To prepare the microporous carbon (MPC)-coated separator (denoted as MPC@PP), microporous bamboo charcoals were first synthesized following the method reported in our previous work.[42] The resulting MPC materials, denoted as *x*-MPC (*x* = 400, 500, and 600), were obtained at different carbonization temperatures (400, 500, and 600 °C) using *P. edulis* bamboo powder as the precursor. The MPC was mixed with conductive carbon and PVDF binder in a mass ratio of 7:2:1 to obtain a uniform slurry, which was then coated onto the PP separator (thickness: 25 μm) and dried overnight before use. The diameter of blank PP and MPC@PP separators was 19 mm in this work.

Characterization Methods

Scanning electron microscopy (SEM) morphology was observed by a JSM-7800F Prime microscope. The element distribution was characterized by an OXFORD X-Max 80 detector. Digital photographs of the lithium polysulfide (Li_2S_8) permeation tests were recorded using H-type cells. The Li_2S_8 solution (0.2 M) was obtained by mixing lithium sulfide and sulfur in DME. Ultraviolet−visible (UV−vis) absorption spectra of the Li_2S_8 solution after 9 h were collected using an UV spectrophotometer (UV-2310 II). Fourier transform infrared spectroscopy (FT-IR) analysis was conducted with a wavenumber from 4000 to 400 cm^{-1}. Lithium symmetric cells were tested at a current density of 0.5 mA cm^{-2} (1 mAh cm^{-2}) at 30 °C. The morphology of cycled lithium anodes was collected by SEM after cycling.

Nyquist plots of all batteries were collected by a potentiostat (CHI660E, CH Instruments) from 1 MHz to 10 mHz with an AC amplitude of 10 mV. Lithium-ion transference number (t_{Li}^+) was measured using the Bruce−Vincent method[43] according to eq 1

$$t_{Li}^+ = I_{ss}(\Delta V - I_o R_o)/I_o(\Delta V - I_{ss}R_{ss}) \quad (1)$$

where ΔV is polarization voltage (10 mV); I_o and I_{ss} are the initial and steady-state current, respectively; and R_o and R_{ss} are the interfacial resistance before and after polarization, respectively.

Battery Measurements

To assemble LCBs, the lithium anode was paired with pristine S (or S@KB, SeS_2@KB) cathode with blank PP (or MPC@PP) as the separator. The ether-based electrolyte composed of 1 M LiTFSI/DOL/DME/$LiNO_3$ (0.2 M) was used in each cell. In this work, the MPC@PP separator faced the cathode side during cell assembly. To unambiguously decouple the influence of the MPC coating on the Li-ion diffusion kinetics within the cathode, a pristine sulfur electrode was employed, whereas the S@KB composite cathode was used to demonstrate the long-term cycling stability achieved by combining physical nanoconfinement with the MPC@PP separator. Cyclic voltammetry (CV) curves were collected using a potentiostat (CHI660E, CH Instruments) from 1.8 to 2.8 V (vs Li/Li^+) at scan rates from 0.04 to 0.10 mV s^{-1}. The Li^+ diffusion coefficient was calculated using the Randles−Ševčík equation (eq S1). Li−S (1C = 1675 mA g^{-1}), Li−S@KB (1C = 1675 mA g^{-1}), and Li−SeS_2@KB

Downloaded from pubs.acs.org/langd5/article-pdf/42/33/24682/6646793/acs.langmuir.6c04214.pdf by SOUTHWEST JIAOTONG UNIV user on 07 November 2026

https://doi.org/10.1021/acs.langmuir.6c04214
Langmuir 2026, 42, 24682−24690

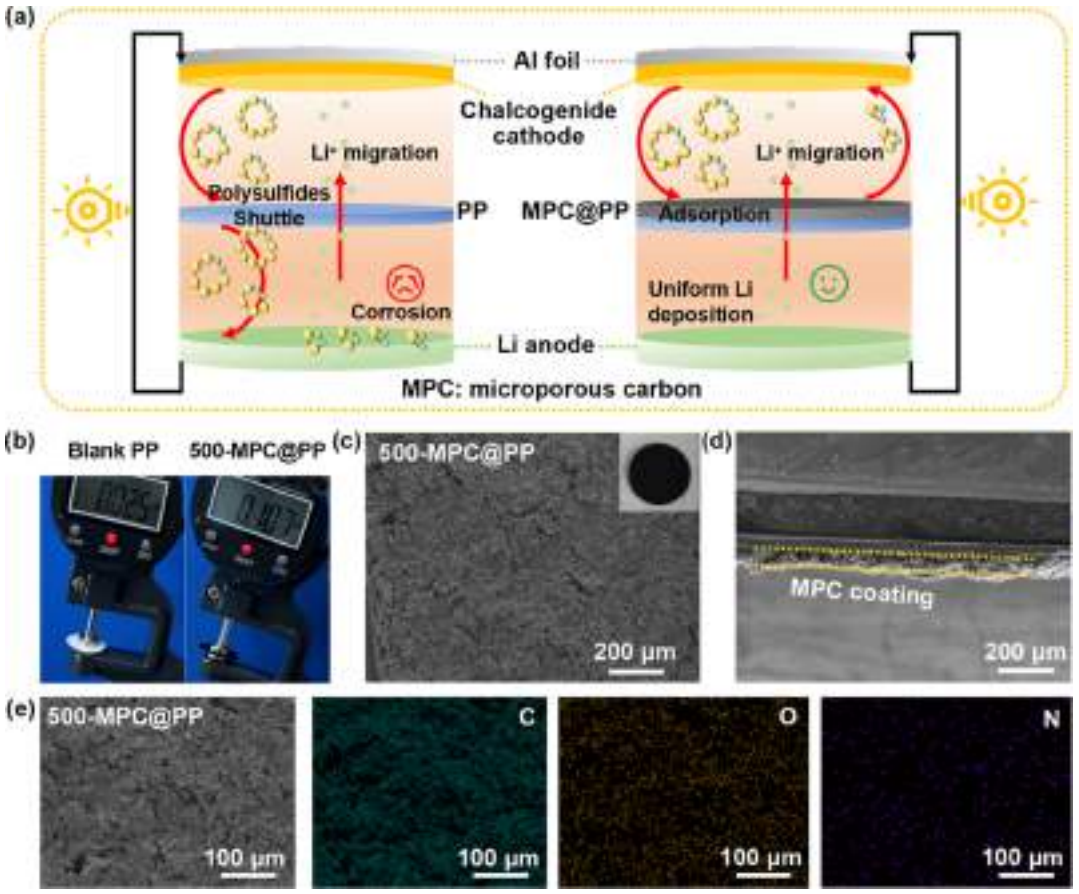


Figure 1. Synthesis and characterization of the MPC@PP separator: (a) schematic profile of lithium−chalcogenide batteries with blank PP and 500-MPC@PP separator; (b) digital photo of blank PP and 500-MPC@PP separator; SEM images of (c) surface and (d) cross section of the 500-MPC@PP separator. The inset shows the digital image of the 500-MPC@PP separator; (e) elemental mapping of C, O, and N of the 500-MPC@PP separator.

cells (1C = 1342 mA g^{-1}) were tested from 1.8 to 2.8 V (vs Li/Li^+) with a NEWARE cycler (CT-4008Tn-5 V10 mA-HWXB) at 25 °C.

RESULTS AND DISCUSSION

Synthesis and Characterization of the MPC@PP Separator

A comparison of the conventional Celgard PP separator and the MPC-modified separator for LCBs is shown in Figure 1a. The blank PP separator shows a porous structure (Figure S1), which allows diffusion of lithium ions and soluble redox-active polysulfides/polyselenides during charging and discharging, leading to a severe shuttle effect in LCBs. Consequently, insoluble Li_2S_2/Li_2S deposits form on the lithium metal anode, exacerbating its passivation and polarization, and leading to irreversible loss of active material and thus capacity decay. To mitigate the shuttle effect caused by these intermediates, an MPC material was synthesized via our previously reported method,[42] which features a pore size of <2 nm, a large pore volume of 1.088 $cm^3\ g^{-1}$ (as previously characterized[42]), and abundant functional groups (e.g., −OH, C═O, and C−O) (Figure S2). This modified separator is denoted as 500-MPC@PP. The 500-MPC@PP separator is designed to trap polysulfides/polyselenides through a combination of physical confinement and chemical adsorption, thereby mitigating the shuttle effect during cycling and further stabilizing the lithium anode upon cycling. Moreover, the 500-MPC@PP separator exhibits improved thermal stability up to 150 °C, whereas the blank PP separator undergoes severe deformation at the same temperature (Figure S3). As shown in Figure 1b−d, the 500-MPC@PP separator has a thickness of 107 μm with a uniform coating layer of 82 μm. Additionally, elemental mapping analysis clearly demonstrates that the target elements are homogeneously enriched on the surface of the 500-MPC@PP separator (Figure 1e).

Electrochemical Measurements of Li−S Batteries with the MPC@PP Separator

The electrochemical performances of Li−S batteries with different separators were examined by assembling coin cells using a pristine sulfur cathode. As shown in Figure 2a,b, two characteristic reduction peaks are observed in the CV curves, corresponding to the conversion of elemental sulfur to soluble polysulfides (Li_2S_n, n = 4, 6, 8) and subsequently to insoluble Li_2S_2/Li_2S, respectively. The oxidation peak is owing to the oxidation of Li_2S_2/Li_2S back to elemental sulfur. Additionally, the Li−S battery with the 500-MPC@PP separator exhibits higher peak currents than that with the blank PP separator, indicating significantly enhanced reaction kinetics. To further evaluate Li^+ diffusion in the Li−S battery containing the 500-MPC@PP separator, the peak currents were fitted and are shown in Figure S4. The Li^+ diffusion coefficient (D_{Li}^+) was calculated by the slope derived from the Randles−Sevčik equation, where a steeper slope indicates faster Li^+ diffusion. As shown in Figure 2c and Table S1, the 500-MPC@PP-based cell shows improved D_{Li}^+ values of 1.67×10^{-8}, 3.64×10^{-8}, and 4.58×10^{-8} $cm^2\ s^{-1}$ for peaks R1, R2, and O, respectively,

https://doi.org/10.1021/acs.langmuir.6c04214
Langmuir 2026, 42, 24682−24690

Downloaded from pubs.acs.org/langd5/article-pdf/42/33/24682/6646793/acs.langmuir.6c04214.pdf by SOUTHWEST JIAOTONG UNIV user on 07 November 2026

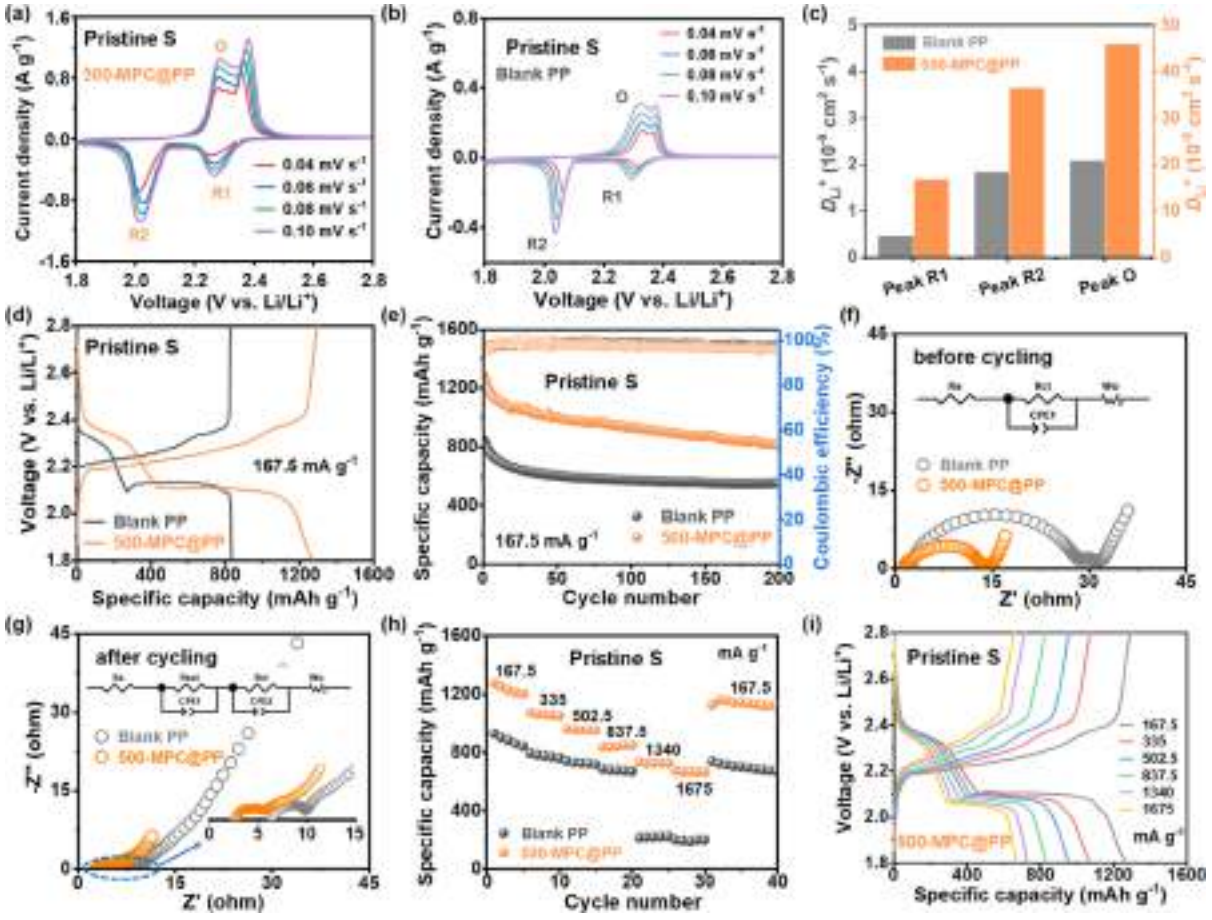


Figure 2. Electrochemical measurement of Li−S batteries with the MPC@PP separator: CV curves of pristine S cathode with (a) 500-MPC@PP and (b) blank PP separator at various scan rates. (c) Comparison of Li^+ diffusion coefficient of pristine S cathode with 500-MPC@PP and blank PP separators. (d) Galvanostatic charge/discharge profiles and (e) cycling performance of Li−S batteries with 500-MPC@PP and blank PP separators at 167.5 mA g^{-1}. Nyquist plots of Li−S batteries with (f) blank PP and (g) 500-MPC@PP separator before and after 200th cycle at the current density of 167.5 mA g^{-1}. (h,i) Rate performance of Li−S batteries with 500-MPC@PP and blank PP separators at current densities from 167.5 to 1675 mA g^{-1}.

which is much higher than those of blank PP cell. These results further demonstrate that the 500-MPC@PP separator accelerates Li^+ diffusivity, owing to the highly porous structure of the 500-MPC material.

To further evaluate the electrochemical properties of the 500-MPC@PP separator, galvanostatic charge−discharge measurements were performed on Li−S batteries with the pristine sulfur cathode (Figure 2d). The Li−S battery incorporating the 500-MPC@PP separator delivers a higher initial capacity of 1277.27 mAh g^{-1} at 167.5 mA g^{-1}, compared to 838.23 mAh g^{-1} for the battery with blank PP. Additionally, the 500-MPC@PP battery exhibits a lower overpotential than the blank PP separator battery, indicating enhanced redox kinetics. After 200 cycles, the 500-MPC@PP cell shows a higher specific capacity than the blank PP cell (Figure 2e), indicating efficient utilization of the active material owing to the MPC coating. Moreover, the 500-MPC@PP cell exhibits much lower interfacial resistance than the blank PP cell both before and after cycling (Figure 2f,g, Tables S1 and S2), which is because of the electrically conductive MPC, leading to fast redox kinetics as previously reported.[44,45] The rate capability of Li−S battery with 500-MPC@PP was further evaluated. As shown in Figure 2h,i, the 500-MPC@PP cell delivers specific capacities of 1274.04, 1073, 958.25, 835.24, 732.55, and 671.99 mAh g^{-1} at current densities from 167.5 to 1675 mAg^{-1}, respectively, which are much higher than those of the blank PP cell at each current density (Figure S5). The significantly improved rate capability of the 500-MPC@PP cell indicates improved utilization of sulfur in the presence of MPC coating, especially at high rates. Additionally, the 500-MPC@PP cell also shows better rate performance than the 400-MPC@PP and 600-MPC@PP cells (Figure S6), which is consistent with the optimal porous structure of 500-MPC as previously reported.[42]

Suppression of Polysulfides Shuttle and Stabilization of Li Metal by the MPC@PP Separator

To further investigate the ability of separator modification to inhibit polysulfide shuttling, we conducted a polysulfide dissolution (Li_2S_8) test using different separators in H-type cells. As shown in Figure 3a,b, the H-cell containing a blank PP separator exhibited a distinct deep yellow color after 9 h, indicating severe polysulfide diffusion through the separator. In contrast, no significant color change was observed for the H-cell with the 500-MPC@PP separator, demonstrating effective suppression of polysulfide diffusion. Furthermore, we quantitatively measured the residual polysulfide content in the right compartment of H cells containing either a blank PP or a 500-MPC@PP separator after 9 h. As shown in Figure 3c, the

https://doi.org/10.1021/acs.langmuir.6c04214
Langmuir 2026, 42, 24682−24690

Downloaded from pubs.acs.org/langd5/article-pdf/42/33/24682/6646793/acs.langmuir.6c04214.pdf by SOUTHWEST JIAOTONG UNIV user on 07 November 2026

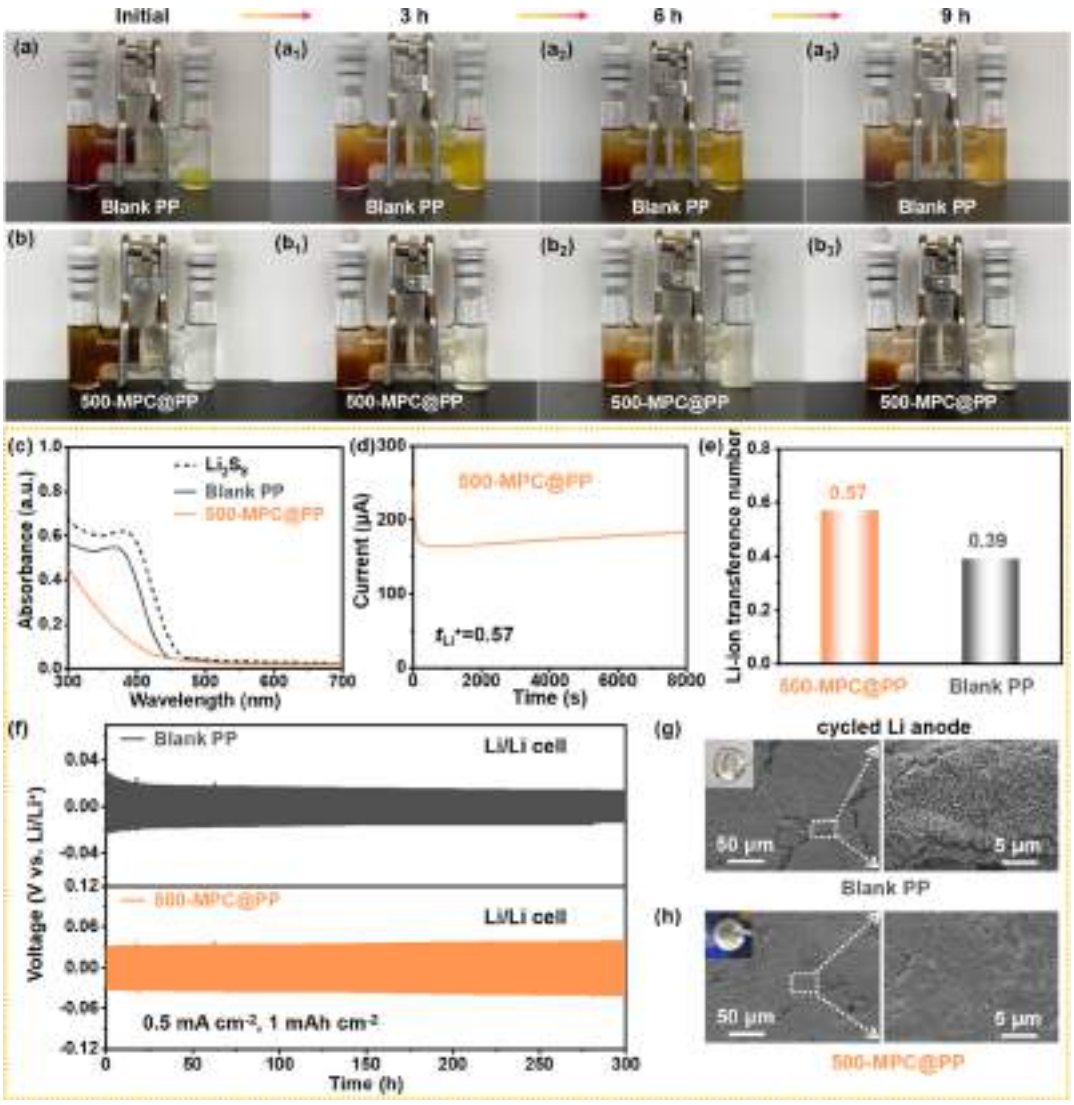


Figure 3. Electrochemical properties of the MPC@PP separator: digital images of the Li_2S_8 electrolyte with (a–a_3) blank PP and (b–b_3) 500-MPC@PP in H-cell; (c) UV–vis spectra of the Li_2S_8 electrolyte before and after H-cell test with blank PP and 500-MPC@PP; (d) current–time curve of symmetric lithium cell with the 500-MPC@PP separator; (e) lithium-ion transference number of blank PP and 500-MPC@PP separators; (f) lithium plating/stripping behavior of blank PP and 500-MPC@PP separators at 0.5 mA cm^{-2} (1 mAh cm^{-2}); SEM morphology of cycled lithium anode with (g) blank PP and (h) 500-MPC@PP separators after 300 h cycling.

absorbance of remaining polysulfides in the right compartment with the 500-MPC@PP separator was significantly lower than that with the blank PP separator. This superior polysulfide shielding performance can be attributed to physical ion-sieving within the abundant micropores of MPC together with chemical adsorption by surface oxygen-containing functional groups as previously reported.[46,47] Given the abundant oxygen-containing groups on biomass-derived carbons and the ease of heteroatom doping (e.g., N), future work could explore surface functionalization to couple physical ion sieving with chemical polysulfide adsorption for enhanced cycling stability.

To investigate the effect of the MPC coating on lithium-ion transport, we measured the lithium-ion transference number (t_{Li}^+) of cells with the MPC@PP separator (Figures 3d,e, S7 and S8). The cell with the 500-MPC@PP separator exhibited a higher t_{Li}^+ of 0.57, compared to 0.39 for the cell with the blank PP separator, indicating that the introduced MPC coating effectively enhances the Li^+ transport kinetics. Although the coating thickness was fixed in this study to ensure mechanical integrity and uniform coverage, a systematic investigation of the thickness-dependent ionic conductivity and lithium ion transference number would be a meaningful direction for future optimization.

The Li/Li symmetric cell with 500-MPC@PP separator was further evaluated at 0.5 mA cm^{-2} and 1 mAh cm^{-2} (Figure 3f). Both the 500-MPC@PP and blank PP cells showed stable lithium plating/stripping processes with a polarization voltage below 50 mV. However, after cycling, the lithium metal anode cycled with the blank PP separator displayed a rough and porous surface with substantial dendrite accumulation (Figure 3g). However, the cycled lithium anode with 500-MPC@PP maintained a smooth and uniform surface, indicating that 500-MPC modified separator effectively regulates uniform lithium deposition and mitigates lithium dendrite growth.

Cycling and Rate Performances of Li–S@KB Batteries with the MPC@PP Separator

Li–S batteries using a S@KB cathode were assembled and measured to further examine the long cycling performance of

https://doi.org/10.1021/acs.langmuir.6c04214
Langmuir 2026, 42, 24682–24690

Downloaded from pubs.acs.org/langd5/article-pdf/42/33/24682/6646793/acs.langmuir.6c04214.pdf by SOUTHWEST JIAOTONG UNIV user on 07 November 2026

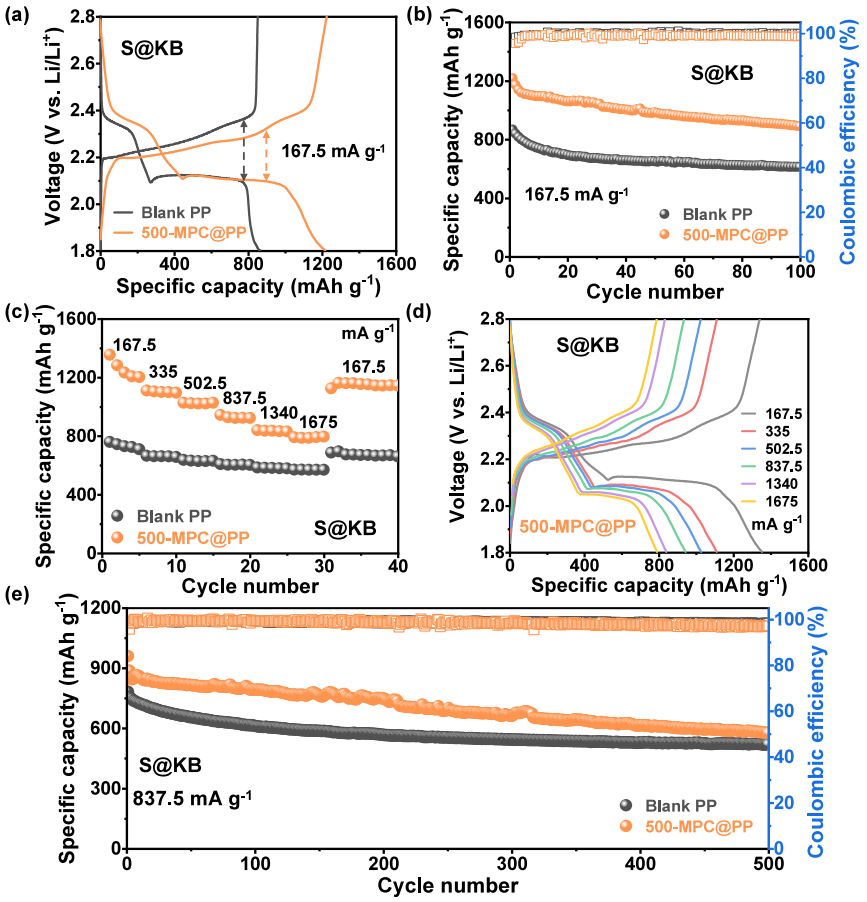


Figure 4. Electrochemical measurement of Li−S@KB batteries with the MPC@PP separator: (a) galvanostatic charge/discharge profiles and (b) cycling performance of Li−S@KB batteries with 500-MPC@PP and blank PP at 167.5 mA g^{-1}. (c,d) Rate performance of Li−S@KB batteries with 500-MPC@PP and blank PP at current densities from 167.5 to 1675 mA g^{-1}. (e) Long cycling performance of Li−S@KB batteries with 500-MPC@PP and blank PP at 837.5 mA g^{-1}.

the 500-MPC@PP separator. As shown in Figure 4a, the 500-MPC@PP cell delivers a much higher initial capacity of 1272.92 mAh g^{-1} at 167.5 mA g^{-1}, compared to 866.88 mAh g^{-1} for blank PP cell, indicating enhanced utilization of active material because of the 500-MPC coating. As presented in Figure 4b, after cycling, the specific capacities decrease to 612.16 mAh g^{-1} for the blank PP cell and 891.21 mAh g^{-1} for the 500-MPC@PP cell. The simultaneous improvement in capacity and cycling stability demonstrates that the 500-MPC modified separator not only mitigates polysulfide diffusion losses but also synergistically enhances interfacial ion transport and reaction kinetics. The comparison of electrochemical performance of reported LCBs with different functional separators is shown in Table S4.

As shown in Figure 4c,d, the Li−S battery with 500-MPC@PP delivers much higher specific capacities of 1111.69, 1027.63, 944.08, 840.28, and 790.74 mAh g^{-1} at 335, 502.5, 837.5, 1340, and 1675 mA g^{-1}, respectively, indicating significantly improved rate capability when compared with the blank PP-based Li−S battery (Figure S9). Additionally, the Li−S battery equipped with the 500-MPC@PP separator exhibits good cycling stability, retaining a high capacity retention over 500 cycles even at 837.5 mA g^{-1} (Figures 4e and S10). Compared to the cell using pristine S cathode, the S@KB cathode with the 500-MPC@PP separator demonstrates much improved electrochemical performance, owing to the physical nanoconfinement provided by the KB host as well as the polysulfide-blocking capability of the 500-MPC coating layer.

Cycling and Rate Performances of Li−SeS_2 Batteries with the MPC@PP Separator

Selenium sulfide (SeS_2) combines the high capacity of sulfur with the good conductivity of selenium, which has been considered as a promising cathode materials. Nevertheless, it also introduces a challenging dual shuttle effect involving polysulfides and polyselenides during cycling. Li−SeS_2 batteries were assembled to evaluate the effectiveness of the separator modification layer in mitigating the shuttle effect. As shown in Figure 5a−c and S11, the 500-MPC@PP cell exhibits an initial reversible capacity of 723.48 mAh g^{-1} at 1342 mA g^{-1} and maintains a specific capacity of 415.18 mAh g^{-1} after 500 cycles with a high average Coulombic efficiency of 99.2%. In contrast, the Li−SeS_2 battery with the blank PP separator shows an initial capacity of 705.61 mAh g^{-1} at 1342 mA g^{-1} and suffers from rapid capacity decay (<300 mAh g^{-1}) after only 100 cycles, which is attributed to the severe and poorly controlled dual shuttle effect under a high current density. Furthermore, the Li−SeS_2 battery with 500-MPC@PP separator shows much higher specific capacities of 829.48, 764.15, 692.05, 635.83, and 602.78 mAh g^{-1} at current densities of 268.4, 402.6, 671, 1073.6, and 1342 mA g^{-1}, respectively, indicating improved rate capability than the battery with blank PP separator (Figure 5d−f). These results

https://doi.org/10.1021/acs.langmuir.6c04214
Langmuir 2026, 42, 24682−24690

Downloaded from pubs.acs.org/langd5/article-pdf/42/33/24682/6646793/acs.langmuir.6c04214.pdf by SOUTHWEST JIAOTONG UNIV user on 07 November 2026

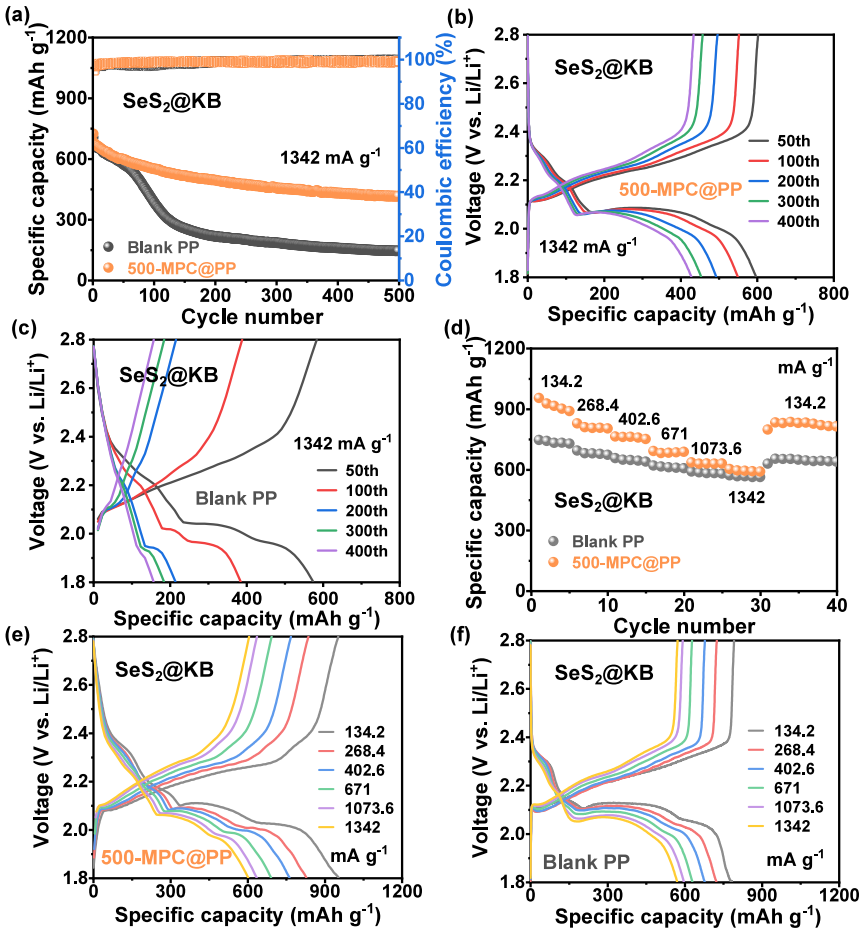


Figure 5. Electrochemical measurement of Li−SeS_2@KB batteries with the MPC@PP separator: (a) cycling performance of Li−SeS_2@KB batteries with 500-MPC@PP and blank PP at 1342 mA g^{-1}. Charge/discharge profiles of Li−SeS_2@KB batteries with (b) 500-MPC@PP and (c) blank PP at 1342 mA g^{-1}. (d) Rate performance of Li−SeS_2@KB batteries with 500-MPC@PP and blank PP at current densities from 134.2 to 1342 mA g^{-1}. Charge/discharge profiles of Li−SeS_2@KB batteries with (e) 500-MPC@PP and (f) blank PP at various current densities.

suggest better utilization of the active material and effective suppression of the intermediate shuttle effect during cycling.

CONCLUSIONS

In summary, this work demonstrates that microporous carbon (MPC), facilely derived from *P. edulis* bamboo, serves as an effective functional interlayer for separators in lithium−chalcogenide batteries, such as Li−S and Li−SeS_2 systems. The as-prepared MPC@PP separator not only physically confines polysulfide/polyselenide species to suppress the shuttle effect but also provides efficient transport pathways for lithium ions. The optimized MPC@PP separator is thus favorable for facilitating Li^+ diffusion while simultaneously blocking polysulfide shuttling. Moreover, this modified separator promotes stable lithium plating/stripping behavior and uniform lithium deposition. Lithium−chalcogenide batteries assembled with the MPC@PP separator exhibit much enhanced cycling stability and rate capability, achieving stable cyclability up to 500 cycles. The stable rate performance achieved in Li−SeS_2 battery further confirms that the 500-MPC interlayer effectively suppresses the dual shuttle effect of both polysulfides and polyselenides. Overall, these findings present a low-cost and practically feasible strategy for fabricating high-performance separators for lithium−chalcogenide batteries, thereby promoting their practical application. This work also offers new insights into the design of biomass-derived functional interlayers for other high-capacity energy storage systems.

ASSOCIATED CONTENT

Supporting Information

The Supporting Information is available free of charge at https://pubs.acs.org/doi/10.1021/acs.langmuir.6c04214.

SEM images of blank PP separator; FT-IR test of 500-MPC; thermal stability of blank PP and 500-MPC@PP; lithium-ion transference number measurements of blank PP and 500-MPC@PP; calculation of diffusion coefficient of Li−S batteries with blank PP and 500-MPC@PP; electrochemical performances of Li−S and Li−SeS_2 batteries with blank PP and 500-MPC@PP; fitting circuit component parameter values of Li−S batteries with PP and 500-MPC@PP; and comparison of electrochemical performances of reported LCBs with different functional separators (PDF)

AUTHOR INFORMATION

Corresponding Authors

Xing Liu − *School of Textile Science and Engineering, Tiangong University, Tianjin 300387, China;* Email: liuxing@tiangong.edu.cn

https://doi.org/10.1021/acs.langmuir.6c04214
Langmuir 2026, 42, 24682−24690

Downloaded from pubs.acs.org/langd5/article-pdf/42/33/24682/6646793/acs.langmuir.6c04214.pdf by SOUTHWEST JIAOTONG UNIV user on 07 November 2026

Weiqing Yang − *Research Institute of Frontier Science, Southwest Jiaotong University, Chengdu 610031, China; Key Laboratory of Advanced Technologies of Materials (Ministry of Education), School of Materials Science and Engineering, Southwest Jiaotong University, Chengdu 610031, China;* orcid.org/0000-0001-8828-9862; Email: wqyang@swjtu.edu.cn

Authors

Panpan Dong − *Research Institute of Frontier Science, Southwest Jiaotong University, Chengdu 610031, China; Key Laboratory of Advanced Technologies of Materials (Ministry of Education), School of Materials Science and Engineering, Southwest Jiaotong University, Chengdu 610031, China;* orcid.org/0000-0002-2349-5988

Ting Yang − *Key Laboratory of Advanced Technologies of Materials (Ministry of Education), School of Materials Science and Engineering, Southwest Jiaotong University, Chengdu 610031, China*

Xuemeng Gan − *Key Laboratory of Advanced Technologies of Materials (Ministry of Education), School of Materials Science and Engineering, Southwest Jiaotong University, Chengdu 610031, China*

Complete contact information is available at: https://pubs.acs.org/10.1021/acs.langmuir.6c04214

Notes

The authors declare no competing financial interest.

■ ACKNOWLEDGMENTS

This work was supported by Sichuan Science and Technology Program (No. 2025ZNSFSC1413), Start-up Research Funding of Southwest Jiaotong University (No. 2682024KJ003), and the Postdoctoral Fellowship Program of China Postdoctoral Science Foundation (No. GZC20241407). The authors are grateful to the Analysis & Testing Center at Southwest Jiaotong University for use of SEM/EDS, FTIR, and UV−vis absorption spectroscopy measurements.

■ REFERENCES

(1) Eftekhari, A. The rise of lithium−selenium batteries. *Sustainable Energy Fuels* **2017**, *1* (1), 14−29.
(2) Xu, G.-L.; Liu, J.; Amine, R.; Chen, Z.; Amine, K. Selenium and Selenium−Sulfur Chemistry for Rechargeable Lithium Batteries: Interplay of Cathode Structures, Electrolytes, and Interfaces. *ACS Energy Lett.* **2017**, *2* (3), 605−614.
(3) Dong, P.; Zhang, X.; Cha, Y.; Lee, J.-I.; Song, M.-K. In situ surface protection of lithium metal anode in Lithium−Selenium disulfide batteries with ionic liquid-based electrolytes. *Nano Energy* **2020**, *69*, 104434.
(4) Cheng, Z.; Wu, P.; Dong, W.-X.; Liu, Z.-P.; Wang, R.-H.; Zhang, T.; Hu, H.; Liu, W.; Chen, L.-F. Biomimetic Gradient-Porous Carbon Enables Sustainable High-Loading Lithium−Sulfur Batteries by Regulating Polysulfide Chemistry. *Angew. Chem., Int. Ed.* **2026**, *65* (22), No. e5836599.
(5) Wang, R.-H.; Guo, H.-N.; Wang, W.; Liu, J.-H.; Hu, L.; Hu, W.; Dong, W.-X.; Chen, L.-F. Crystal Facet Engineering Induces Polarization Electric Fields to Improve the Overall Performance of Lithium−Sulfur Batteries. *ACS Nano* **2025**, *19* (48), 41158−41171.
(6) Dong, W.-X.; Wu, P.; Hu, L.; Guo, H.-N.; Qian, J.-W.; Chen, L.-F.; Yu, S.-H. Hierarchical Pore Carbon Nanocages Embedding with CoTe as Sulfur Host: Synergistic Mass Transfer and Polysulfides Catalytic Conversion in Lithium−Sulfur Batteries. *CCS Chem.* **2026**, *8* (4), 1937−1951.
(7) Pham, V. H.; Boscoboinik, J. A.; Stacchiola, D. J.; Self, E. C.; Manikandan, P.; Nagarajan, S.; Wang, Y.; Pol, V. G.; Nanda, J.; Paek, E.; Mitlin, D. Selenium-sulfur (SeS) fast charging cathode for sodium and lithium metal batteries. *Energy Storage Mater.* **2019**, *20*, 71−79.
(8) Yari, S.; Conde Reis, A.; Pang, Q.; Safari, M. Performance benchmarking and analysis of lithium-sulfur batteries for next-generation cell design. *Nat. Commun.* **2025**, *16* (1), 5473.
(9) Raza, H.; Bai, S.; Cheng, J.; Majumder, S.; Zhu, H.; Liu, Q.; Zheng, G.; Li, X.; Chen, G. Li-S Batteries: Challenges, Achievements and Opportunities. *Electrochem. Energy Rev.* **2023**, *6* (1), 29.
(10) Martinez-Cisneros, C.; Antonelli, C.; Levenfeld, B.; Varez, A.; Sanchez, J. Y. Evaluation of polyolefin-based macroporous separators for high temperature Li-ion batteries. *Electrochim. Acta* **2016**, *216*, 68−78.
(11) Choi, J.; Kim, P. J. A roadmap of battery separator development: Past and future. *Curr. Opin. Electrochem.* **2022**, *31*, 100858.
(12) Gering, K. L. Prediction of Electrolyte Conductivity: Results from a Generalized Molecular Model Based on Ion Solvation and a Chemical Physics Framework. *Electrochim. Acta* **2017**, *225*, 175−189.
(13) Fong, K. D.; Self, J.; Diederichsen, K. M.; Wood, B. M.; McCloskey, B. D.; Persson, K. A. Ion Transport and the True Transference Number in Nonaqueous Polyelectrolyte Solutions for Lithium Ion Batteries. *ACS Cent. Sci.* **2019**, *5* (7), 1250−1260.
(14) Zhou, P.; Zhang, X.; Xiang, Y.; Liu, K. Strategies to enhance Li + transference number in liquid electrolytes for better lithium batteries. *Nano Res.* **2023**, *16* (6), 8055−8071.
(15) Chen, M.; Shao, M.; Jin, J.; Cui, L.; Tu, H.; Fu, X. Configurational and structural design of separators toward shuttling-free and dendrite-free lithium-sulfur batteries: A review. *Energy Storage Mater.* **2022**, *47*, 629−648.
(16) Xiang, H.; Deng, N.; Zhao, H.; Wang, X.; Wei, L.; Wang, M.; Cheng, B.; Kang, W. A review on electronically conducting polymers for lithium-sulfur battery and lithium-selenium battery: Progress and prospects. *J. Energy Chem.* **2021**, *58*, 523−556.
(17) Song, X.; Wang, S.; Chen, G.; Gao, T.; Bao, Y.; Ding, L.-X.; Wang, H. Fe-N-doped carbon nanofiber and graphene modified separator for lithium-sulfur batteries. *Chem. Eng. J.* **2018**, *333*, 564−571.
(18) Wang, Y.; Yang, L.; Chen, Y.; Li, Q.; Chen, C.; Zhong, B.; Guo, X.; Wu, Z.; Wang, G. Novel Bifunctional Separator with a Self-Assembled FeOOH/Coated g-C3N4/KB Bilayer in Lithium−Sulfur Batteries. *ACS Appl. Mater. Interfaces* **2020**, *12* (52), 57859−57869.
(19) Guo, H.-N.; Dong, W.-X.; Fang, Z.-Y.; Hu, L.; Chen, J.; Chen, L.-F. Nitrogen-Doped Graphene/Cellulose Fibers Double-Coated Asymmetric Separator for High-Performance Lithium-Sulfur Batteries. *Adv. Sustainable Syst.* **2025**, *9* (4), 2401047.
(20) Wang, J.; Li, J. C@MoS2 modified separator as efficient trapper and catalysis for promoting polysulfide conversion in Li-S battery. *J. Colloid Interface Sci.* **2022**, *616*, 298−303.
(21) Xie, F.; Xu, C.; Song, Y.; Liang, Q.; Ji, J.; Wang, S. 2D-2D heterostructure of ionic liquid-exfoliated MoS2/MXene as lithium polysulfide barrier for Li-S batteries. *J. Colloid Interface Sci.* **2023**, *636*, 528−536.
(22) Chen, H.; Xiao, Y.; Chen, C.; Yang, J.; Gao, C.; Chen, Y.; Wu, J.; Shen, Y.; Zhang, W.; Li, S.; Huo, F.; Zheng, B. Conductive MOF-Modified Separator for Mitigating the Shuttle Effect of Lithium−Sulfur Battery through a Filtration Method. *ACS Appl. Mater. Interfaces* **2019**, *11* (12), 11459−11465.
(23) Jin, H.-G.; Wang, M.; Wen, J.-X.; Han, S.-H.; Hong, X.-J.; Cai, Y.-P.; Li, G.; Fan, J.; Chao, Z.-S. Oxygen Vacancy-Rich Mixed-Valence Cerium MOF: An Efficient Separator Coating to High-Performance Lithium−Sulfur Batteries. *ACS Appl. Mater. Interfaces* **2021**, *13* (3), 3899−3910.
(24) Zhou, C.; Dong, C.; Wang, W.; Tian, Y.; Shen, C.; Yan, K.; Mai, L.; Xu, X. An ultrathin and crack-free metal-organic framework film for effective polysulfide inhibition in lithium−sulfur batteries. *Interdiscip. Mater.* **2024**, *3* (2), 306−315.

Downloaded from pubs.acs.org/langd5/article-pdf/42/33/24682/6646793/acs.langmuir.6c04214.pdf by SOUTHWEST JIAOTONG UNIV user on 07 November 2026

(25) Gu, J.; Dong, C.; Zhu, Y.; Liu, H.; Ji, J.; Yu, Y.; Ma, C.; Zhou, C.; Mai, L.; Xu, X. Constructing Matching Interfaces by Amorphous Engineering for Enhanced Lithium Ion Transport in Quasi-Solid-State Lithium−Iodine Batteries. *Angew. Chem.* **2025**, *137* (29), No. e202507184.
(26) Si, L.; Wang, J.; Li, G.; Hong, X.; Wei, Q.; Yang, Y.; Zhang, M.; Cai, Y. High energy density lithium-selenium batteries enabled by a covalent organic framework-coated separator. *Mater. Lett.* **2019**, *246*, 144−148.
(27) Xu, N.; Hu, Y.; Sun, B.; Xie, W.; Yao, C.; Xu, Y.; Qi, J. Highly Electronegative Element-Rich COF Modified Separator Achieves High-Performance of Lithium−Sulfur Batteries. *ACS Appl. Polym. Mater.* **2024**, *6* (22), 13813−13818.
(28) Versaci, D.; Canale, I.; Goswami, S.; Amici, J.; Francia, C.; Fortunato, E.; Martins, R.; Pereira, L.; Bodoardo, S. Molybdenum disulfide/polyaniline interlayer for lithium polysulphide trapping in lithium-sulphur batteries. *J. Power Sources* **2022**, *521*, 230945.
(29) Yang, M.; Nan, J.; Chen, W.; Hu, A.; Sun, H.; Chen, Y.; Wu, C. Interfacial engineering of polypropylene separator with outstanding high-temperature stability for highly safe and stable lithium-sulfur batteries. *Electrochem. Commun.* **2021**, *125*, 106971.
(30) Zhang, J.; Yang, H.; Zhu, X.; Zhang, T.; Shu, X.; Liu, C.; Cao, C. C.; Xu, G.; Zhu, M. Enhanced Lithium-Ion Transport and Sulfur Conversion Kinetics in Li−S Batteries via High-Dielectric Composite Separators. *Nano Lett.* **2025**, *25* (25), 9935−9943.
(31) Liu, H.; Liu, C.; Zhou, Y.; Zhang, Y.; Deng, W.; Zou, G.; Hou, H.; Ji, X. The application of Al2O3 in separators and solid electrolytes of lithium-ion battery: A review. *Energy Storage Mater.* **2024**, *71*, 103575.
(32) Chen, L.; Yu, H.; Li, W.; Dirican, M.; Liu, Y.; Zhang, X. Interlayer design based on carbon materials for lithium−sulfur batteries: a review. *J. Mater. Chem. A* **2020**, *8* (21), 10709−10735.
(33) Gao, L.; Wang, X.; Cao, Q.; Jing, B. Geometric design of carbon-based interlayer for advanced lithium-sulfur batteries. *J. Energy Storage* **2024**, *96*, 112661.
(34) Zhang, K.; Wang, L.; Cai, W.; Chen, L.-F.; Wang, D.; Chen, Y.; Pan, H.; Wang, L.; Qian, Y. Pyridinic and pyrrolic nitrogen-enriched carbon as a polysulfide blocker for high-performance lithium−sulfur batteries. *Inorg. Chem. Front.* **2019**, *6* (4), 955−960.
(35) Choi, Y.; Jang, H.; Kim, J.-P.; Lee, J.; Jeong, E. D.; Bae, J.-S.; Shin, H.-C. Porous Carbon Interlayer Derived from Traditional Korean Paper for Li−S Batteries. *Nanomaterials* **2024**, *14*, 385.
(36) Srikhaow, A.; Mensing, J. P.; Lohitkarn, J.; Sriprachuabwong, C.; Poochai, C.; Choominjak, Y.; Wisitsoraat, A.; Lomas, T.; Tuantranont, A. Improved Performance of Lithium−Sulfur Batteries Using Nitrogen-Doped Reduced Graphene Oxide-Coated Separators with Optimized Nitrogen Content. *Energy Fuels* **2022**, *36*, 13902−13910.
(37) Jo, S.; Hong, J.-W.; Momma, T.; Park, Y.; Heo, J.; Park, J.-W.; Ahn, S. Facile one-pot synthesis of biomass-derived activated carbon as an interlayer material for a BAC/PE/Al2O3 dual coated separator in Li−S batteries. *RSC Adv.* **2023**, *13* (39), 27274−27282.
(38) Kang, X.; He, T.; Niu, S.; Zhang, J.; Zou, R.; Zhu, F.; Ran, F. Precise Design of a 0.8 nm Pore Size in a Separator Interfacial Layer Inspired by a Sieving Effect toward Inhibiting Polysulfide Shuttling and Promoting Li+ Diffusion. *Nano Lett.* **2024**, *24* (33), 10007−10015.
(39) Pavlenko, V.; Khosravi H, S.; Żółtowska, S.; Haruna, A. B.; Zahid, M.; Mansurov, Z.; Supiyeva, Z.; Galal, A.; Ozoemena, K. I.; Abbas, Q.; Jesionowski, T. A comprehensive review of template-assisted porous carbons: Modern preparation methods and advanced applications. *Mater. Sci. Eng. R Rep.* **2022**, *149*, 100682.
(40) Lamastra, F. R.; Bragaglia, M.; Paleari, L.; Nanni, F.; Fabborcino, F.; Scarselli, M. Form-Stable Phase-Change Materials Using Chemical Vapor Deposition-Derived Porous Supports: Carbon Nanotube/Diatomite Hybrid Powder and Carbon Nanotube Sponges. *Materials* **2024**, *17* (23), 5721.
(41) Romero, C.; Liu, Z.; Wei, Z.; Fei, L. A review of hierarchical porous carbon derived from various 3D printing techniques. *Nanoscale* **2024**, *16* (26), 12274−12286.
(42) Yang, T.; Dong, P.; Chen, Z.; Gan, X.; Gu, L.; Lin, Q.; Yang, W. Phyllostachys Edulis-Derived Nanoconfined Microporous Carbon−Sulfur Cathodes for High-Rate Lithium−Sulfur Batteries. *ACS Appl. Mater. Interfaces* **2025**, *17* (47), 64677−64686.
(43) Evans, J.; Vincent, C. A.; Bruce, P. G. Electrochemical measurement of transference numbers in polymer electrolytes. *Polymer* **1987**, *28* (13), 2324−2328.
(44) Yao, S.; Liu, H.; Zhang, C.; Zhang, W.; Ma, C.; Rehman, Z. U.; Shen, X. Enhanced polysulfides conversion with hybrid bipolar membrane composed of CoSe2 and amide-functionalized CNTs composites for lithium sulfur batteries. *J. Energy Storage* **2024**, *78*, 110087.
(45) Indubala, E.; Zhao, Y.; Narayanan, N.; Yao, S. Spinel zinc-cobalt oxide porous nanorod combined with reduced graphene oxide as an efficient cathode material for lithium-sulfur batteries. *J. Energy Storage* **2026**, *150*, 120571.
(46) Li, C.; Zhang, W.; Zhang, C.; Ma, C.; Yao, S. Structural evolution and sodium storage behaviors of hollow vs solid hard carbon nanofibers for high-rate sodium ion batteries. *Sustainable Mater. Technol.* **2026**, *48*, No. e02038.
(47) Chen, Y.; Zhang, C.; Li, C.; Gao, T.; Li, Y.; Jiang, Y.; Niu, J.; Zhang, M.; Yao, S. Enhanced Polysulfide Immobilization and Conversion Enabled by N/O/P Co-Doped Hollow Carbon Nanofibers Hosts in Room-Temperature Na-S Batteries. *Carbon* **2026**, *251*, 121354.

Downloaded from pubs.acs.org/langd5/article-pdf/42/33/24682/6646793/acs.langmuir.6c04214.pdf by SOUTHWEST JIAOTONG UNIV user on 07 November 2026

https://doi.org/10.1021/acs.langmuir.6c04214
Langmuir 2026, 42, 24682−24690